Journal of Physics:
Conference Series

PURPOSE-LED PUBLISHING™

PAPER • **OPEN ACCESS**

Integration of High-Temperature Heat Pumps in Industrial Nut Roasting: Psychrometric Assessment for Exhaust Waste Heat Recovery Application and Primary Energy Requirement Reduction

To cite this article: Saverio Mirandola *et al* 2026 *J. Phys.: Conf. Ser.* **3351** 012034

View the article online for updates and enhancements.

You may also like

- Testing coffee roasting machine with electric heater as energy source
Syafriandi, F Fachruddin, A Lubis et al.
- Physicochemical and Functional Characteristics of Roasted Sticky Rice Flour (Tapuang Bareh Randang) in Various Methods
C W Refdi, W S Murtius and P Y Fajri
- Effects of roasting and NH_4Cl catalysis on the direct electrotransformation products from an $AlCl_3$ solution
Xiuxiu Han, Ting-an Zhang, Guozhi Lv et al.

Enabling Electrochemistry Inside and Outside the Lab

PalmSens

Discover our diverse range of Potentiostats engineered to support your research wherever it takes you

- Intuitive software for Windows and Android
- Proven in over 4000 scientific publications
- Single-channel and multi-channel
- Benchtop, portable and wearable

Discover More



This content was downloaded from IP address 79.13.44.163 on 18/11/2026 at 18:39

Journal of Physics: Conference Series **3351** (2026) 012034 doi:10.1088/1742-6596/3351/1/012034

Integration of High-Temperature Heat Pumps in Industrial Nut Roasting: Psychrometric Assessment for Exhaust Waste Heat Recovery Application and Primary Energy Requirement Reduction

Saverio Mirandola[1], Lorenzo Ruini[2], Paolo E. Santangelo[2,3], Alberto Muscio[4]

[1]VUORMAR Packaging s.r.l., Via Don Sturzo 13, 37060 Correzzo (VR) Italy
[2]Dipartimento di Scienze e Metodi dell'Ingegneria, Università degli Studi di Modena e Reggio Emilia, Via G. Amendola 2, 42122 Reggio Emilia, Italy
[3]Centro Interdipartimentale per la Ricerca Applicata e i Servizi nel Settore della Meccanica Avanzata e della Motoristica dell'Università degli Studi di Modena e Reggio Emilia - InterMech MO.RE., Via P. Vivarelli 10, 41125 Modena, Italy
[4]Dipartimento di Ingegneria "Enzo Ferrari", Università degli Studi di Modena e Reggio Emilia, Via P.Vivarelli 10, 41125 Modena (MO), Italy

[1]Email: saverio_mirandola@vuormar.it

Abstract. Industrial hot-air dry roasting in the nut processing sector is characterized by high specific thermal energy consumption and significant low energy efficiency ratio, mainly due to direct air heating and limited recovery of waste heat from exhaust streams. This study investigates the work condition design and integration of a high temperature heat pump system for waste heat recovery and process air preheating in an industrial gas-fed hot-air roasting plant; Moreover it aims to evaluate the complete replacing of traditional thermal source with heat pump use through a required primary energy reduction. The hot and humid exhaust air flow from the drying section is directed onto the heat exchanger of a high temperature heat pump. Both sensible and most important latent heat are then recovered to keep the cold sink of the heat pump warm enough to reduce the temperature leap from the two heat sinks, thus optimizing the size of the compressor to eventually increase the COP of the system. A dry roaster case study is considered and two temperature interval scenarios are evaluated. R1233zd_e is considered as the main refrigerant fluid due to its versatility and current state of the art commercial use. Optimal refrigerant mass flow rate is then evaluated in relation to the nut roasting process requirements. The investigation aims to lead to a significant attention raise in high temperature heat pump use for medium temperature application (below 200°C) such as roasting where a hot and humid exhaust flow rate is available throughout the production cycle due to the main task of the process itself: decrease moisture from the main product that is eventually exhausted and available outside the drying/roasting chamber. The study underlines that, under the considered fluid and process assumptions, it is possible to recover from approximately 33 % to about 39 % of the burner thermal demand at the hot sink — depending on whether the heat pump is designed for a conservative (T_{cond} = 80 °C) or frontier (T_{cond} = 110 °C) condensation temperature,

and accounting for air-side heat-exchanger efficiencies of 0.90. This pre-heating effect reduces the natural gas consumption and, when the compressor is supplied by an on-site photovoltaic plant in self-consumption, leads to an overall specific primary-energy reduction of approximately 65 Wh/kg of inlet product against a baseline thermal-energy requirement of about 168 Wh/kg derived from process assumptions for industrial hazelnut dry-roasting.

Keywords: Dry Roasting, Heat Pump, Psychrometric, Refrigerant fluid, Waste Heat

1. Introduction

Medium-temperature industrial process heat (100–200 °C) is one of the hardest segments of the European energy transition, accounting for about 27% of the industrial thermal demand [1, 2]. Food processing, and in particular drying and roasting, is among the most energy-intensive uses, since heat is traditionally supplied by natural-gas combustion through direct or indirect hot-air heaters [3]. Two structural features drive the low efficiency: single-pass combustion of the heat carrier, and the discharge of a warm, moisture-laden exhaust whose latent and sensible enthalpy is rarely recovered [4].

Dry nut roasting is representative of this paradigm. The process couples moisture reduction (drying) with chemical-organoleptic development (roasting), with hot-air setpoints of 130–180 °C and inlet moisture contents of 5–10% depending on the product [5, 6]. The exhaust leaves the chamber at temperatures close to or above the drying setpoint and carries an absolute humidity several times higher than ambient, making it a high-quality low-grade waste-heat source currently dispersed to the atmosphere.

HTHP technology has matured rapidly. Units delivering 90–120 °C are commercially available, while research-stage systems target 150–200 °C, often based on low-GWP refrigerants such as R1233zd(E), R1336mzz(Z) and R601 (n-pentane) [7, 8, 9]. Performance is governed by the temperature lift between source and sink: minimising this lift while securing the required sink temperature is the design priority for the COP. In drying applications, intercepting the latent heat of the moist exhaust lets the evaporator work near or below the dew point, effectively raising the source temperature and enabling competitive COP values in the medium-temperature range [10, 11].

Despite this potential, the literature on HTHP integration in nut roasting is scarce. Most works address drying in dairy, paper or textile industries [12, 13], where the exhaust latent content is higher but the target temperatures are lower. The combination of medium-high targets (∼150 °C), modulated moisture and intermittent operation typical of nut processing has not been systematically assessed. Moreover, rising gas prices, ETS allowances in energy costs and the diffusion of photovoltaic (PV) self-consumption open a new scenario in which electrifying process heat through HTHPs can become both feasible and economically attractive [14, 15].

Independent assessments by the IEA Heat Pumping Technologies programme report energy savings up to 30% when HTHPs recover exhaust heat and pre-heat make-up air in food drying [30], confirming the order of magnitude targeted here.

The approach is as follows. A reference nut roaster is defined, and an HTHP is sized to recover the sensible and latent enthalpy from the drying exhaust and pre-heat the process air. Two temperature scenarios are evaluated, R1233zd(E) is adopted as the main refrigerant, and a sensitivity analysis is run over refrigerant type and condensation temperature. The latent-

recovery mechanism is captured through an effective specific heat of the humid exhaust. Finally, the primary-energy savings and avoided CO_2 emissions are quantified for two electricity supplies: the Italian grid and on-site PV self-consumption.

2. Materials and methods

2.1 Process description and reference case study

The dry-roasting process comprises three phases: drying (product from ambient to approx. 80 °C, moisture from 8% to 3%), roasting (up to approx. 150 °C, moisture down to 1%) and cooling back to ambient [5, 16]. Drying and roasting occur in the same hot-air column; the main carrier is process air heated by a gas burner (mainly Natural gas or LPG). Its thermal efficiency is set to $\eta_b = 0.90$, a representative value for indirect gas-fired air heaters [17], and the sensible-and-latent transfer efficiency to the product to $\eta_{a\to p} = 0.70$, consistent with the range reported for convective nut roasters [16].

Hazelnut is the reference product, with specific heat 1700 J/(kg·K) and density 660 kg/m^3 taken from the ASHRAE food-property tables and the FAO/INFOODS database [18, 19]. Mass and energy balances are written per kilogram of inlet product, making the derived indicators independent of roaster size and directly comparable with other industrial cases. The reference parameters are summarised in Tables 1-3; the process assumptions and phase subdivision (Tables 1-3) are adapted from the authors' previous work [31] under CC-BY 4.0 licence.

Table 1. Main Roasting Product Assumption (adapted from [31] under CC-BY 4.0)

Product	Density	Specific Heat
Hazelnuts	660 kg/m^3	1700 J/(kgK)

Table 2. Main Roasting Process Assumptions (adapted from [31] under CC-BY 4.0)

Property	Value
Drying Max Temperature [4,8,10]	80 °C
Saturation Vapor pressure	47,5 kPa
Roasting Max Temperature [4,8,10]	150 °C
Saturation Vapor pressure	490,2 kPa
Inlet Moisture Content	8 %
Outlet Moisture Content	1 %
Burner/Heater heat exchange efficiency	90%
Hot air/Product heat exchange efficiency	70%

Table 3. Main Roasting Process Subdivision (adapted from [31] under CC-BY 4.0)

Drying Phase		
Property	Inlet	Outlet
Temperature	20 °C	80 °C
Moisture Content	8 %	3 %
Roasting Phase		
Property	Inlet	Outlet

Temperature	80 °C	150 °C
Moisture Content	3 %	1 %
Cooling Phase		
Property	Inlet	Outlet
Temperature	150 °C	40 °C
Moisture Content	1 %	1 %

From Tables 1–3, the overall thermal demand per kilogram of inlet product is the sum of the sensible heat raising the product temperature in each phase and the latent heat evaporating the corresponding moisture, as in Eq. (1). The primary energy at the burner follows from Eq. (2). With the reference values, $q_{useful} \approx 105$ Wh/kg and $q_{burner} \approx 168$ Wh/kg, obtained directly from the process assumptions summarised in Tables 1-3.

$$q_{useful} = \Sigma_i \left[c_{p,p} \cdot \Delta T_i + \Delta MC_i \cdot h_{fg} \right] \quad (1)$$

$$q_{burner} = q_{useful} / \left(\eta_b \cdot \eta_{a \to p} \right) \quad (2)$$

A water-vapour mass balance gives the absolute humidity of the exhaust, Eq. (3). Assuming all moisture removed from the product is carried by the process air, for the reference case (ΔMC_{tot} = 7%, ambient UA_{amb} = 7.25 g/kg_{da} at 20°C and 50% RH, air-to-product ratio 2.4 kg_{da}/kg_p) it is found UA_{exh} = 36.4 g/kg_{da} with a dew point T_{dew} = 35.1 °C. The assumed intake state (20°C, 50% RH) corresponds to standard indoor design conditions for moist-air calculations [20]. These reference case assumptions values are based on experimental evidence from current roasting plants. These data are investigated in their bounded set. In following studies, backwards sensitivity analysis could be performed on these parameters to further investigate their correlation. The air-to-product ratio is an operating figure of the roasting plants considered in this study, set so that the resulting exhaust humidity and temperature reproduce their measured operating envelope. T_{dew} sets the lower bound of the evaporator temperature in the cycle model.

$$UA_{exh} = UA_{amb} + \left(\dot{m}_p \cdot \Delta MC_{tot} \right) / \dot{m}_{da} \quad (3)$$

2.2 HTHP integration concept

The HTHP is installed in the existing gas-fired roaster as follows. The hot, humid exhaust from the drying chamber is routed to the HTHP evaporator, where it is cooled and partially dehumidified down to a temperature compatible with the refrigerant pinch. The recovered sensible and latent enthalpy is upgraded by the cycle and delivered at the condenser to the incoming fresh air, which is pre-heated. A residual gas burner then raises the pre-heated air to the 150 °C roasting setpoint. Figure 1 shows the integration layout.

Commercial gas-to-liquid plate heat exchangers designed for exhaust heat recovery, such as the Alfa Laval GL/GLH series [29], suit this duty: they provide integrated gas/condensate separation, low gas-side pressure drop and design temperatures above the present requirements.

In this configuration the HTHP acts as a thermal multiplier over a resistive system: per unit of electrical input it delivers COP units of heat at the condenser, against one for a resistance heater. This multiplication is decisive when the electricity comes from PV self-consumption, where the avoided primary energy approaches the full condenser duty.

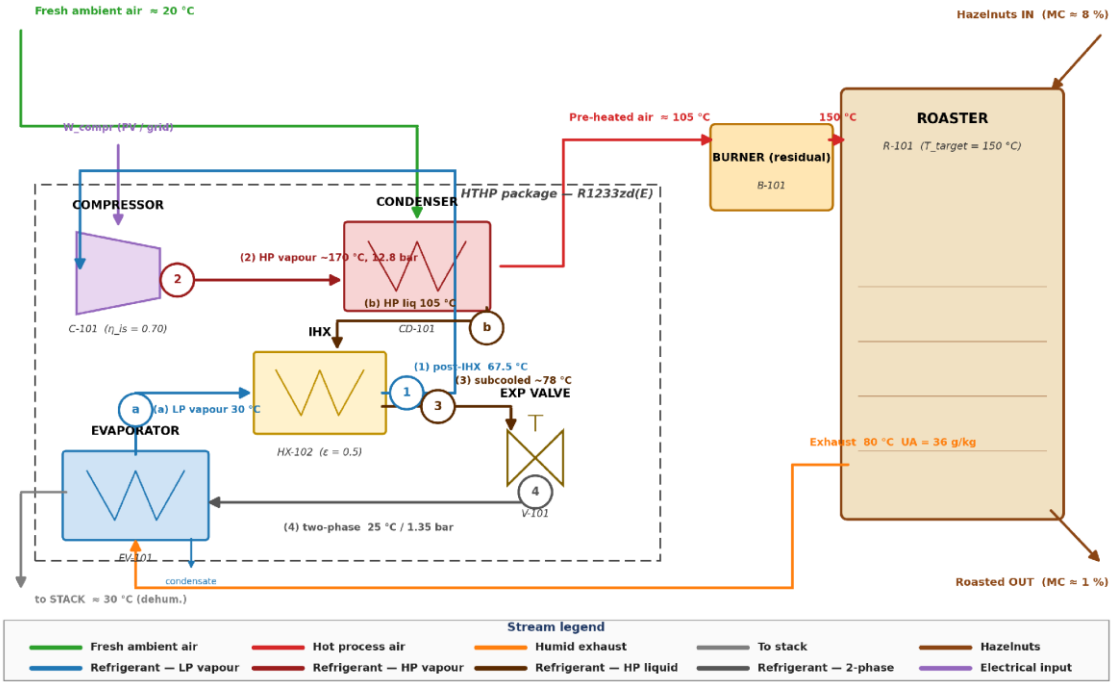

Figure 1. P&ID-style schematic of the HTHP-integrated industrial nut-roasting plant.

2.3 Psychrometric modelling of the exhaust side

The state of the humid exhaust is computed with the ideal-gas model of moist air [20]. The saturation pressure of water vapour is evaluated with a Magnus-type exponential correlation in the simplified form widely adopted in psychrometric and meteorological practice [22], Eq. (4); the absolute humidity follows from Eq. (5) and the moist-air specific enthalpy per kilogram of dry air from Eq. (6). Over the 20-110 °C range spanned by the exhaust stream, Eq. (4) agrees with the ASHRAE reference formulation [20] to within 0.5 % and the resulting dew-point temperature differs by less than 0.1 K – both well within the uncertainty of the other model parameters.

$$p_{sat}(T) = 611 \cdot 10^{7.5 \cdot T / (237.7 + T)} \quad [Pa] \qquad (4)$$

$$UA = 0.622 \cdot p_v / (p_{atm} - p_v) \qquad (5)$$

$$h = 1.005 \cdot T + UA \cdot (2501 + 1.86 \cdot T) \quad [kJ/kg_{da}] \qquad (6)$$

Latent recovery is central. Below T_{dew} the vapour condenses, releasing latent enthalpy and steepening the h(T) curve. This is captured by an effective specific "virtual" heat of the humid air, defined as the ratio of total enthalpy variation to temperature variation along the cooling path, Eq. (7). For the reference scenario (UA_{exh} = 36.4 g/kg_{da}, cooling from 80 °C to 30 °C) it reaches 1.56 kJ/(kg·K), about 55% above the dry-air value, with roughly 31% of the recovered enthalpy from latent condensation.

$$c_{p,virt} = [h(T_{in}, UA_{in}) - h(T_{out}, UA_{out})] / (T_{in} - T_{out}) \qquad (7)$$

2.4 HTHP cycle modelling

A single-stage subcritical vapour-compression cycle is adopted. An Internal Heat Exchanger (IHX), widely recommended for medium- and high-temperature heat pumps [10], is included. The cycle has five characteristic points: saturated vapour leaving the evaporator (a), superheated vapour entering the compressor (1), superheated vapour delivered at the condenser (2), saturated/subcooled liquid leaving the condenser (b) and subcooled liquid entering the expansion valve (3).

The IHX exchanges heat between the high-pressure subcooled liquid and the low-pressure saturated vapour: it lowers h_3, reducing the flash-gas fraction at the valve, and raises h_1, slightly increasing the discharge enthalpy. Its effectiveness is set to $\varepsilon_{IHX} = 0.5$, a conservative value for coaxial IHX in HFO/HCFO systems [10].

The energy balances at the evaporator, condenser and compressor are given by Eqs. (8), (9) and (10), where h_{2s} is the isentropic discharge enthalpy and $\eta_{is} = 0.70$ the isentropic efficiency, representative of scroll/screw compressors at the pressure ratios investigated [9]. Evaporator and condenser pinch constraints, $\Delta T_{pinch} = 5$ K [8], close the system. Two air-side heat-exchanger efficiencies, $\eta_{HX,evap} = \eta_{HX,cond} = 0.90$, account for the non-ideal transfer between refrigerant and air streams; typical of industrial finned-tube and plate-and-fin coils [10, 29], they scale the air-side duties and reduce the system-level coverage without affecting the cycle COP. The COP is defined by Eq. (11).

$$\dot{Q}_{evap} = \dot{m}_{ref} \cdot (h_a - h_4) \quad (8)$$

$$\dot{Q}_{cond} = \dot{m}_{ref} \cdot (h_2 - h_b) \quad (9)$$

$$\dot{W}_{compr} = \dot{m}_{ref} \cdot (h_{2s} - h_1) / \eta_{is} \quad (10)$$

$$COP = \dot{Q}_{cond} / \dot{W}_{compr} \quad (11)$$

Two design points represent the currently available commercial HTHP ranges. The first, $T_{cond} = 80$ °C, is the conservative configuration, aligned with medium-high temperature units on the European market (Carrier 61CW-Z, hot water up to 90 °C, operated here at 80 °C to limit the lift). The second, $T_{cond} = 110$ °C, is the frontier configuration, aligned with recent ultra-high-temperature units (Carrier 61CWD, envelope up to 120 °C [28], operated at 110 °C to keep the pressure ratio below the scroll/screw limit). Both share $T_{evap} = 25$ °C and the IHX-augmented layout. Figure 2 reports the T–s diagram of the cycle for both the conservative (80 °C) and frontier (110 °C) design points, highlighting the different condensation levels and compression works.

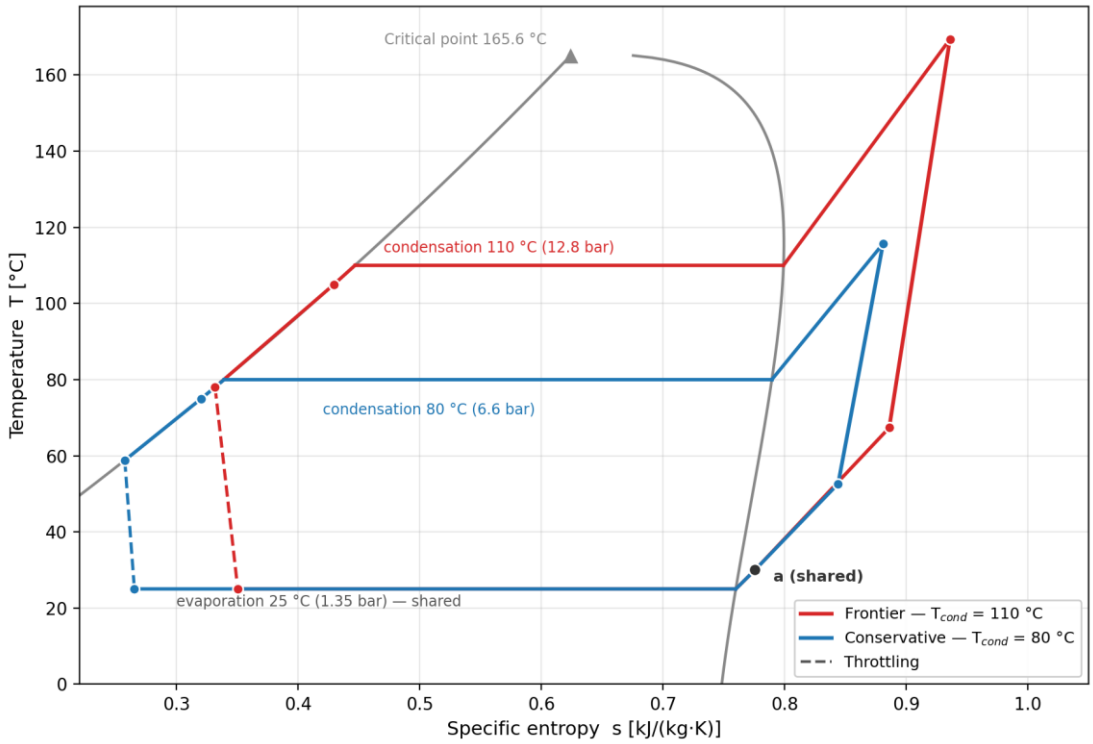

Figure 2. T–s diagram of the R1233zd(E) HTHP cycle for the conservative (condensation at 80 °C) and frontier (condensation at 110 °C) design points; both share the evaporation at 25 °C and the IHX-augmented layout.

The refrigerant mass flow is obtained by inverting the evaporator balance once the available evaporator duty is fixed from the exhaust psychrometric balance, Eq. (12). Refrigerant properties are evaluated through the Wagner-4 vapour-pressure equation and the Watson-Riedel latent-heat correlation [23, 24], with constants from the equations of state of [7] for R1233zd(E), [8] for R1336mzz(Z) and the NIST WebBook for R601 [25].

$$\dot{m}_{ref} = \dot{Q}_{evap}{}^{air} / (h_a - h_4) \quad (12)$$

2.5 Refrigerant selection criteria

R1233zd(E) is the reference fluid, chosen for: a critical temperature of 165.6 °C [7], leaving margin above the design condensation temperature; negligible GWP (=1); A1 safety class (non-toxic, non-flammable); and current commercial availability for HTHPs [9]. R1336mzz(Z) and R601 are retained as comparators for the sensitivity analysis.

Commercial readiness of R1233zd(E) at the design point is supported by recent industrial water-source units rated up to 120 °C heat-sink temperature, with 110–540 kW nominal heating capacity (Carrier 61CWD [28]), targeting the process- and district-heating segments addressed here.

2.6 Primary-energy and PV self-consumption modelling

$$SPES = Q_{cond,useful} - W_{compr} \cdot PEF_{el} \quad [Wh/kg_p] \quad (13)$$

Integration with an on-site PV plant in self-consumption is included as a supporting economic-environmental scenario. The primary energy of the HTHP electrical input is $W_{compr} \cdot PEF_{el}$. Two cases are considered: grid supply, PEF_{el} = 1.95 [21], for the average 2026 Italian mix; and PV self-consumption, $PEF_{el} \approx 0$, treating PV electricity as primary-energy-free at generation [26]. The specific primary-energy saving (SPES) follows from Eq. (13).

The replacing factor, i.e. the burner-duty fraction replaceable by the HTHP, is amplified by the COP: each kWh of PV electricity delivers COP kWh of heat, partly offsetting the higher specific CAPEX of the HTHP over a resistance heater.

3. Results

3.1 Psychrometric balance of the exhaust airstream

Two exhaust temperatures are evaluated, a high ($T_{exh,in}$ = 80 °C) and a reduced ($T_{exh,in}$ = 60 °C) drying regime of the same plant. Both share the dry-air mass ratio and thus UA_{exh} = 36.4 g/kg_{da} and T_{dew} = 35.1 °C; only the inlet temperature changes, giving inlet RH of 11.9% at 80 °C and 28.4% at 60 °C (Figure 3).

Cooling to 30 °C (RH ≈ 100%) yields a recoverable enthalpy of 77.4 kJ/kg_{da} on the 80–30 °C path (sensible 69%, latent 31%) and 56.5 kJ/kg_{da} on the 60–30 °C path (sensible 58%, latent 42%). The effective specific heat of the humid air is 1.56 kJ/(kg·K) for the high regime and 1.88 kJ/(kg·K) for the reduced one, respectively 55% and 87% above the dry-air value.

Per kg of inlet product (air-to-product ratio 2.4 kg_{da}/kg_p following process assumptions), the theoretical recoverable evaporator duty is about 51.6 Wh/kg_p for the high regime and 37.3 Wh/kg_p for the reduced one. After the non-ideal exhaust-to-refrigerant exchange ($\eta_{HX,evap}$ = 0.90), the heat actually absorbed drops to about 46.5 and 33.6 Wh/kg_p respectively.

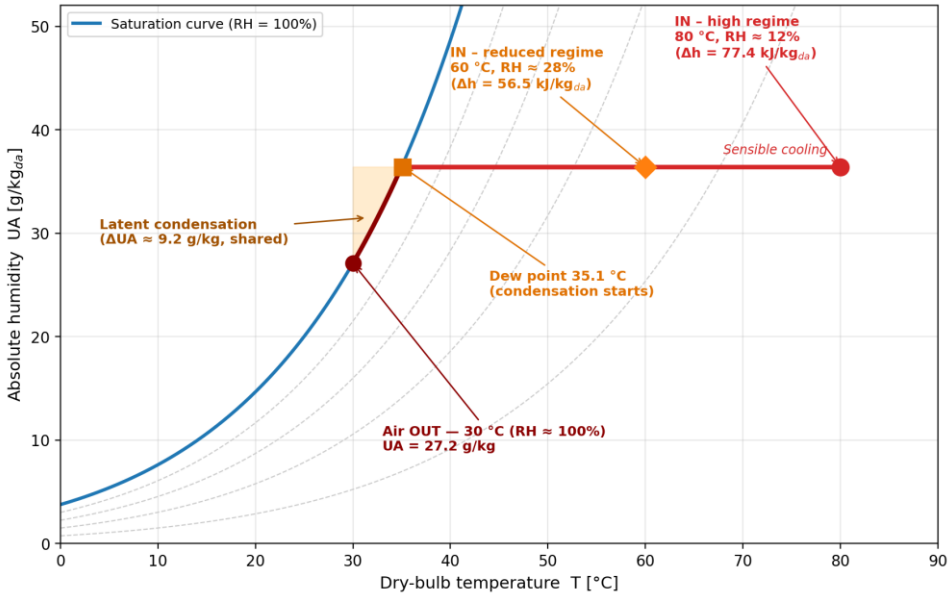

Figure 3. Exhaust-air evolution on the psychrometric chart for the two drying regimes (inlet at 80 °C and 60 °C): sensible cooling at constant humidity down to the shared dew point (35.1 °C), followed by partial condensation along the saturation line.

3.2 R1233zd(E) cycle performance — dual scenario

The cycle is computed under the reference assumptions T_{evap} = 25 °C, i.e. 5 K below the 30 °C air-outlet temperature, which is itself about 5 K below T_{dew}, so that latent recovery is enabled; superheating and subcooling of 5 K; IHX effectiveness 0.5; isentropic efficiency 0.70 [9, 10]; and air-side efficiencies $\eta_{HX,evap}$ = $\eta_{HX,cond}$ = 0.90 (§2.4). Figure 4 shows the resulting evaporator temperature profiles and the pinch location.

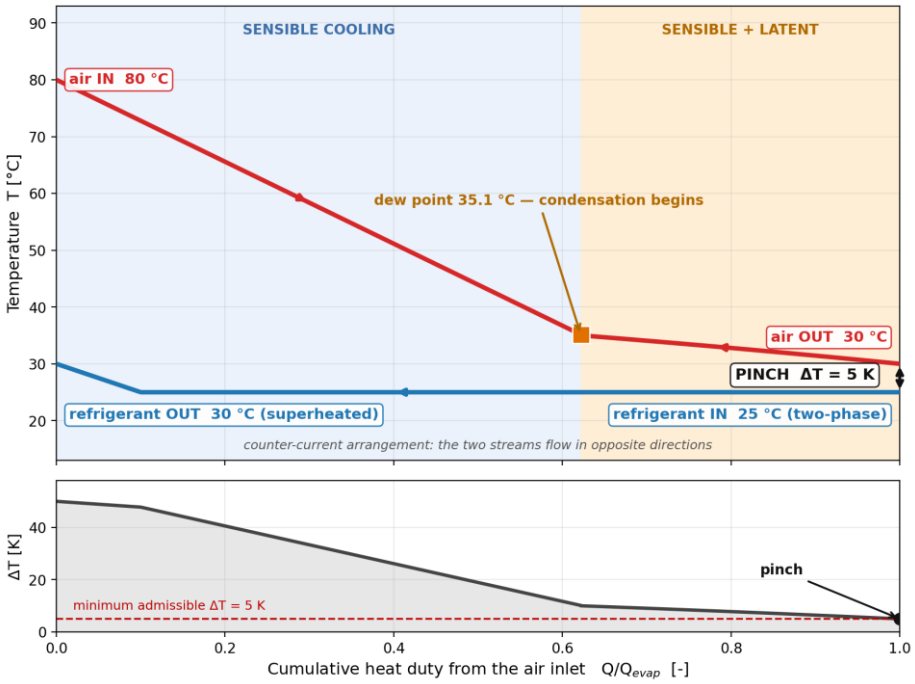

Figure 4. Evaporator temperature–duty diagram (counter-current): exhaust air cooling from 80 °C to 30 °C against R1233zd(E) evaporating at 25 °C. The upper plot shows the sensible and the sensible-plus-latent

zones separated by the dew point; the lower plot shows the temperature difference between the two streams along the exchanger, with the pinch (ΔT = 5 K) at the air-outlet end.

At the frontier point (T_{cond} = 110 °C, ΔTlift = 85 K), the cycle gives COP = 2.78, pressure ratio 9.5 and a refrigerant mass flow of about 1320 kg/h at the 1000 kg/h of net product roasting reference plant. The condenser duty delivered to the fresh air is about 65 Wh/kg_p, i.e. 38.9% of the baseline burner consumption, with a compressor input of about 26 Wh/kg_p; the corresponding suction volumetric flow, about 200 m^3/h, falls within the commercial range of HFO scroll/screw compressors at this capacity (Carrier 61CWD [28]). Under PV supply (PEF_{el} ≈ 0) the SPES approaches 65 Wh/kg_p, a ~39% reduction over the gas baseline; under grid supply (PEF_{el} = 1.95) it falls to about 8.6%, confirming PV integration as the decisive factor.

At the conservative point (T_{cond} = 80 °C, ΔT_{lift} = 55 K, PR = 4.9), the cycle gives COP = 4.21, a refrigerant mass flow of about 1100 kg/h at the 1000 kg/h of net product roasting reference plant, a condenser duty of about 55 Wh/kg_p (32.7% of baseline) and a compressor input of about 14.5 Wh/kg_p. Under PV the SPES approaches 55 Wh/kg_p (32.7%); under grid supply it falls to about 27 Wh/kg_p (15.9%). The conservative point has a higher COP and a larger absolute grid saving, but covers a smaller hot-side fraction, since the burner must still bridge from 80 °C to the 150 °C target.

As a second-law benchmark, $COP_{Carnot} = T_{cond}/(T_{cond} - T_{evap})$ is 6.42 for the conservative and 4.51 for the frontier configuration. The cycle COPs of 4.21 and 2.78 thus correspond to exergetic efficiencies of about 66% and 62%, within the range reported for industrial subcritical HTHPs [4, 9] and confirming the model as a realistic target rather than an idealised bound.

3.3 Sensitivity on the condensation temperature

A sensitivity analysis over T_{cond} in 110–130 °C, other assumptions fixed, gives a COP decreasing almost linearly from 2.78 at 110 °C to 2.26 at 130 °C, while the pressure ratio rises from 9.5 to 14.1. The condenser fraction increases mildly (from about 39% to 45%) as the higher q_{cond} per unit mass offsets the COP penalty. The grid primary-energy saving falls from 8.6% to about 1.9%, limited by the critical-temperature margin of R1233zd(E). The trade-off between delivery temperature and cycle efficiency identifies T_{cond} ≈ 110 °C as the design sweet-spot (Figure 5), in line with the frontier configuration.

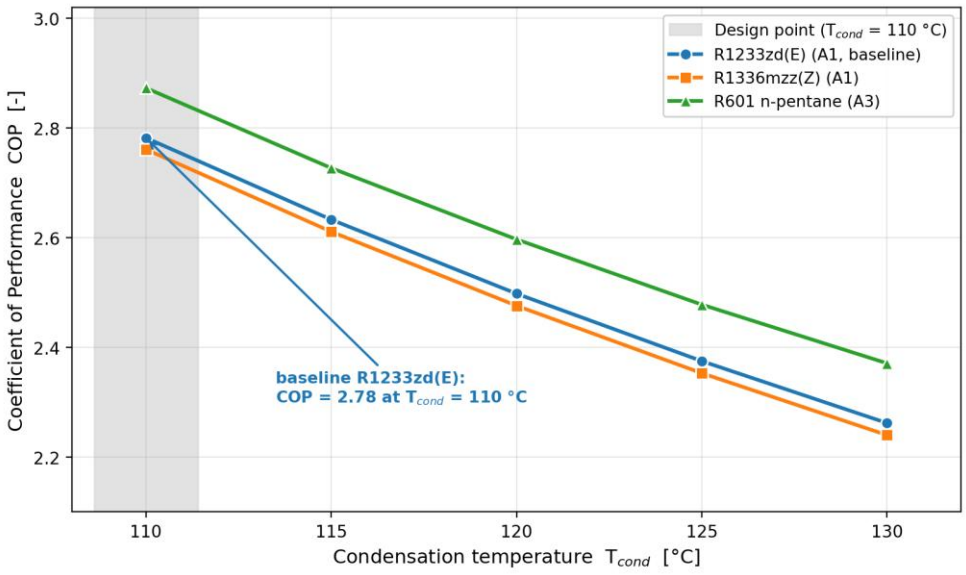

Figure 5. COP sensitivity vs T_{cond} for the three refrigerants (T_{evap} = 25 °C, IHX active, η_{is} = 0.70).

3.4 Refrigerant comparison

Two alternative refrigerant fluids are considered as benchmarks. R1336mzz(Z) gives COP = 2.76, essentially equal to R1233zd(E) (2.78), but with a higher pressure ratio (11.1 vs 9.5) and a larger critical-temperature margin (61 K), making it a viable A1 alternative above 130 °C. R601 (n-pentane) reaches the highest COP (2.87) thanks to its high latent heat, but its A3 class (flammable) requires ATEX installation [9], limiting it to large plants, as in the 4 MW pentane HTHP at the Tiense Suiker refinery [27]. At the case-study scale, R1233zd(E) remains the pragmatic baseline.

4. Discussion: economic and environmental supporting analysis

The simulations confirm that the HTHP recovers about 33–39% of the burner thermal demand at the hot sink. Translating this into primary-energy saving depends critically on the electricity source. With the 2026 Italian grid (PEF_{el} = 1.95 [21]) the compressor primary energy offsets much of the gas saved, leaving a net reduction of about 9% at the frontier and 16% at the conservative point. With on-site PV self-consumption ($PEF_{el} \approx 0$ [26]) the COP-multiplier effect is fully translated into avoided primary energy, giving a SPES of about 65 Wh/kg_p, a ~39% reduction over the gas baseline.

In emissions terms, the gas baseline is about 33 g_{CO2}/kg_p; the HTHP+PV configuration cuts this to about 20 g_{CO2}/kg_p, an avoided ~13 g_{CO2}/kg_p, equal to about 77 t_{CO2}/year for a 1000 kg/h plant running 6000 h/year.

A simplified levelized cost of heat (LCOH) is evaluated for three configurations. With Italian industrial market figures, the LCOH is about 72 €/MWh_{th} for the gas baseline, about 88 €/MWh_{th} for HTHP from the grid and about 61 €/MWh_{th} for HTHP from PV self-consumption, the latter alone undercutting the gas baseline (Figure 6).

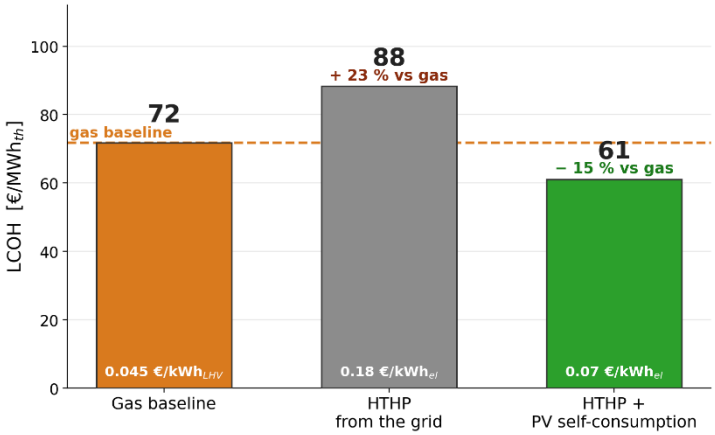

Figure 6. Levelized Cost of Heat (LCOH) comparison for the three supply configurations.

The dual-scenario approach (conservative T_{cond} = 80 °C vs frontier T_{cond} = 110 °C) reveals a trade-off relevant to equipment selection. The conservative configuration uses widely available hardware at low pressure ratio (PR ≈ 5) and high COP (~4.2) but leaves a large residual burner duty between 80 °C and the 150 °C target. The frontier configuration aligns with recent ultra-high-temperature units (R1233zd(E), envelope up to 120 °C [28]), cutting the residual gas demand at a lower COP (~2.8) and higher pressure ratio (PR ≈ 9.5).

The choice depends on the relative cost of gas and electricity, on PV availability, on the required decarbonisation depth and on further considerations according to the objectives of the financial feasibility of the HTHP installation related to the roasting process (mainly Net Positive

Value and Internal Rate of Return considerations that could be furtherly investigated in following studies).

5. Conclusions

A HTHP based on the low-GWP refrigerant R1233zd(E) was sized and analysed for the recovery of sensible and latent waste heat from the moist exhaust of an industrial nut roaster. On a specific-mass basis and accounting for air-side efficiencies $\eta_{HX,evap} = \eta_{HX,cond} = 0.90$, the system delivers about 33–39% of the burner thermal demand at the condenser, i.e. about 65 Wh/kg of inlet product, at COP = 2.78 under the reference conditions (T_{evap} = 25 °C, T_{cond} = 110 °C, IHX active). The exhaust latent content proved decisive in keeping the evaporator temperature high, yielding an effective specific heat up to about 1.6 times the dry-air value in the high regime.

The sensitivity analysis over T_{cond} (110–130 °C) and refrigerant (R1336mzz(Z), R601) showed differences below 5% on COP and identified the electricity source as the dominant economic-environmental driver: the HTHP becomes competitive only with on-site PV self-consumption, giving a primary-energy saving of about 39% and avoided emissions of about 77 t_{CO2}/year for a 1000 kg/h plant. R1233zd(E) is confirmed as the pragmatic baseline, with R1336mzz(Z) as an A1 alternative for slightly higher T_{cond} and R601 as the high-COP natural option under ATEX constraints.

Future work will model the dynamic off-design behaviour and integrate thermal storage to decouple PV generation from process operation. A more detailed assessment of cascade or transcritical configurations for higher delivery temperatures could further extend the applicability of the proposed solution.

Acknowledgments

During the preparation of this work the authors used Claude (Anthropic, Opus 4 model) for language readability improvement of author-written text, for generating the figures from the authors' own calculation model, and for final proof-checking. All numerical results presented in this paper were produced by the authors' own thermodynamic model, and all the cited references were verified by the authors against the original sources. The authors reviewed and edited the output and take full responsibility for the content of this publication.

References

[1] Rightor E., Scheihing P., Hoffmeister A., Papar R. Industrial Heat Pumps: Electrifying Industry's Process Heat Supply. Report IE2201, American Council for an Energy-Efficient Economy, Washington DC, 2022. https://www.aceee.org/research-report/ie2201

[2] Marina A., Spoelstra S., Zondag H.A., Wemmers A.K. An estimation of the European industrial heat pump market potential. Renewable and Sustainable Energy Reviews, vol. 139, 110545, 2021. https://doi.org/10.1016/j.rser.2020.110545

[3] International Energy Agency. The Future of Heat Pumps – Analysis. IEA, Paris, 2023. https://www.iea.org/reports/the-future-of-heat-pumps

[4] Arpagaus C., Bless F., Uhlmann M., Schiffmann J., Bertsch S.S. High temperature heat pumps: Market overview, state of the art, research status, refrigerants, and application potentials. Energy, vol. 152, pp. 985-1010, 2018. https://doi.org/10.1016/j.energy.2018.03.166

[5] Perren R., Escher F.E. Impact of roasting on nut quality. In: Improving the Safety and Quality of Nuts, Woodhead Publishing, pp. 173-197, 2013. https://doi.org/10.1533/9780857097484.2.173

[6] Bagheri H. Application of Infrared Heating for Roasting Nuts. Journal of Food Quality, 8813047, 2020. https://doi.org/10.1155/2020/8813047
[7] Mondéjar M.E., McLinden M.O., Lemmon E.W. Thermodynamic Properties of trans-1-Chloro-3,3,3-trifluoropropene (R1233zd(E)): Vapor Pressure, (p, rho, T) Behavior, Speed of Sound Measurements, and Equation of State. Journal of Chemical & Engineering Data, vol. 60, pp. 2477-2489, 2015. https://doi.org/10.1021/acs.jced.5b00348
[8] McLinden M.O., Akasaka R. Thermodynamic Properties of cis-1,1,1,4,4,4-Hexafluorobutene [R-1336mzz(Z)]: Vapor Pressure, (p, ρ, T) Behavior, and Speed of Sound Measurements and Equation of State. Journal of Chemical & Engineering Data, vol. 65, no. 9, pp. 4201-4214, 2020. https://doi.org/10.1021/acs.jced.9b01198
[9] Bamigbetan O., Eikevik T.M., Neksa P., Bantle M., Schlemminger C. Theoretical analysis of suitable fluids for high temperature heat pumps up to 125 degC heat delivery. International Journal of Refrigeration, vol. 92, pp. 185-195, 2018. https://doi.org/10.1016/j.ijrefrig.2018.05.017
[10] Navarro-Esbrí J., Mota-Babiloni A. Experimental analysis of a high temperature heat pump prototype with low global warming potential refrigerant R-1336mzz(Z) for heating production above 155 degC. International Journal of Thermofluids, vol. 17, 100304, 2023. https://doi.org/10.1016/j.ijft.2023.100304
[11] Wang J.F., Brown C., Cleland D.J. Heat pump heat recovery options for food industry dryers. International Journal of Refrigeration, vol. 86, pp. 41-50, 2018. https://doi.org/10.1016/j.ijrefrig.2017.11.028
[12] Zühlsdorf B., Bühler F., Bantle M., Elmegaard B. Analysis of technologies and potentials for heat pump-based process heat supply above 150 degC. Energy Conversion and Management: X, vol. 2, 100011, 2019. https://doi.org/10.1016/j.ecmx.2019.100011
[13] Minea V. Drying heat pumps - Part I: System integration. International Journal of Refrigeration, vol. 36, no. 3, pp. 643-658, 2013. https://doi.org/10.1016/j.ijrefrig.2012.11.025
[14] Eurostat. Energy statistics - prices of natural gas and electricity for industrial consumers. European Commission, 2025. https://ec.europa.eu/eurostat/databrowser/view/nrg_pc_203
[15] International Energy Agency. Real-time Electricity Tracker. IEA, 2025. https://www.iea.org/data-and-statistics/data-tools/real-time-electricity-tracker
[16] Riggi R., Modesti M., Alfieri G., Esposito G., Cucchiara P., Ferri S., Mencarelli F., Bellincontro A. Integration of Destructive and Non-Destructive Analytical Determinations for Evaluating Quality of Fresh and Roasted Hazelnuts Subjected to Different Processing Temperatures. Food Science & Nutrition, vol. 13, e70095, 2025. https://doi.org/10.1002/fsn3.70095
[17] UNI/TS 11300-1:2014. Prestazioni energetiche degli edifici - Parte 1: Determinazione del fabbisogno di energia termica dell'edificio per la climatizzazione estiva ed invernale. Ente Italiano di Normazione, 2014.
[18] ASHRAE. ASHRAE Handbook - Refrigeration (SI), Chapter 8: Thermal Properties of Foods. American Society of Heating, Refrigerating and Air-Conditioning Engineers, Atlanta, 2002.
[19] Charrondière U.R., Haytowitz D., Stadlmayr B. FAO/INFOODS Density Database Version 2.0. Food and Agriculture Organization, Rome, 2012. https://www.fao.org/infoods/
[20] ASHRAE. ASHRAE Handbook - Fundamentals (SI). American Society of Heating, Refrigerating and Air-Conditioning Engineers, Atlanta, 2017.
[21] Ministero dello Sviluppo Economico. Decreto 26 giugno 2015 - Applicazione delle metodologie di calcolo delle prestazioni energetiche e definizione delle prescrizioni e dei requisiti minimi degli edifici, Allegato 2: Fattori di conversione in energia primaria. Gazzetta Ufficiale Serie Generale n. 162, 2015.
[22] World Meteorological Organization. Guide to Meteorological Instruments and Methods of Observation. WMO-No. 8, 7th edition, Geneva, 2008.
[23] Reid R.C., Prausnitz J.M., Poling B.E. The Properties of Gases and Liquids. 5th edition, McGraw-Hill, New York, 2001.
[24] Watson K.M. Thermodynamics of the Liquid State - Generalized Prediction of Properties. Industrial & Engineering Chemistry, vol. 35, no. 4, pp. 398-406, 1943. https://doi.org/10.1021/ie50400a004
[25] NIST. Chemistry WebBook - n-Pentane Thermophysical Properties. NIST Standard Reference Database Number 69, National Institute of Standards and Technology, 2024. https://webbook.nist.gov/chemistry/
[26] GSE - Gestore dei Servizi Energetici. Ritiro Dedicato e autoconsumo fotovoltaico: modalità di accesso e indicatori di prestazione. 2024. https://www.gse.it/servizi-per-te/fotovoltaico/ritiro-dedicato
[27] European Heat Pump Association. Sweet and sustainable: new heat pump at sugar factory. EHPA News, 2025. https://ehpa.org/news-and-resources/news/sweet-and-sustainable-new-heat-pump-at-sugar-factory/
[28] Carrier Corporation. 61CWD Ultra High Temperature Series - Product Selection Data, doc. 10775_PSD_08/2023. Carrier S.C.S., 2023.
[29] Alfa Laval. GL150 / GLH150 Gas-to-liquid Plate Heat Exchanger – Product Leaflet, doc. 200001678-6-EN-GB. Alfa Laval AB, Lund. https://assets.alfalaval.com/documents/p699b6e49/alfa-laval-gl150-glh150-product-leaflet-en.pdf

[30] IEA Heat Pumping Technologies. Annex 58 - High-Temperature Heat Pumps. Final Report, International Energy Agency Technology Collaboration Programme on Heat Pumping Technologies, 2023. https://heatpumpingtechnologies.org/annex58/
[31] Mirandola S., Puglia M., Muscio A., Tartarini P. Efficiency Enhancement in Dry Roasting Processes Using Hybrid Gas-Electric Powered Thermal Sources: A Case Study in Nut Processing. Journal Européen des Systèmes Automatisés, vol. 58, no. 9, art. 580915, 2025. https://doi.org/10.18280/jesa.580915

Nomenclature

Latin symbols

c_p	specific heat at constant pressure, kJ/(kg·K)
$c_{p,p}$	specific heat of the product, J/(kg·K)
$c_{p,l}$	specific heat of the saturated liquid refrigerant, kJ/(kg·K)
$c_{p,v}$	specific heat of the saturated vapour refrigerant, kJ/(kg·K)
$c_{p,virt}$	effective (virtual) specific heat of the humid exhaust air, kJ/(kg·K)
COP	coefficient of performance (cycle), –
h	specific enthalpy, kJ/kg
h_a, h_b	specific enthalpy at evaporator outlet (a) and condenser outlet (b), kJ/kg
h_1, h_2, h_3, h_4	specific enthalpy at the four characteristic points of the HTHP cycle, kJ/kg
h_{2s}	isentropic compressor discharge specific enthalpy, kJ/kg
h_{fg}	latent heat of vaporization, kJ/kg
$LCOH$	levelized cost of heat, €/MWh$_{th}$
$\dot{m}_p$	product mass flow rate, kg/s
$\dot{m}_{da}$	dry-air mass flow rate, kg/s
$\dot{m}_{ref}$	refrigerant mass flow rate, kg/s
$\dot{m}_w$	mass flow rate of water evaporated from the product, kg/s
MC_{in}, MC_{out}	product moisture content at inlet/outlet of the process, kg/kg
ΔMC	difference of moisture content, kg/kg
p	pressure, Pa or bar
p_{sat}	saturation pressure of water vapour, Pa
p_v	partial pressure of water vapour in moist air, Pa
p_{atm}	atmospheric pressure, Pa
p_{evap}, p_{cond}	evaporation and condensation pressure of the refrigerant, bar
PEF_{el}	primary energy factor of the electricity supply, –
PR	compressor pressure ratio = p_{cond} / p_{evap}, –
q_{useful}	thermal energy delivered to the product per kg of inlet product, Wh/kg$_p$
q_{burner}	primary thermal energy supplied at the burner per kg of inlet product, Wh/kg$_p$
q_{cond}	specific condenser heat duty (per kg refrigerant or per kg product), kJ/kg or Wh/kg$_p$
$q_{evap,air}$	evaporator heat duty taken from the exhaust air per kg of inlet product, Wh/kg$_p$
$\dot{Q}_{evap}$, $\dot{Q}_{cond}$	evaporator and condenser heat rate, kW
s	specific entropy, kJ/(kg·K)
$SPES$	specific primary-energy saving, Wh/kg$_p$
T	temperature, °C or K
T_{evap}, T_{cond}	saturation temperature of refrigerant at evaporator/condenser, °C
T_{dew}	dew-point temperature of the moist exhaust airstream, °C

T_{NBP}	normal boiling point of the refrigerant (at 1.013 bar), °C or K
T_{crit}	critical temperature of the refrigerant, °C or K
UA	absolute humidity (moisture mass ratio) of the air, kg_w/kg_{da}
UA_{amb}, UA_{exh}	absolute humidity of ambient and exhaust air, kg_w/kg_{da}
UR	relative humidity, –
$\dot{w}_{compr}$	specific compressor work (per kg refrigerant or per kg product), kJ/kg or Wh/kg_p
$\dot{W}_{compr}$	compressor electrical power, kW

Greek symbols

ΔT_{lift}	temperature lift of the cycle = $T_{cond} - T_{evap}$, K
ΔT_{pinch}	pinch point temperature difference on heat exchangers, K
ΔT_{sup}	superheating at compressor suction, K
ΔT_{sub}	subcooling at condenser outlet, K
ε_{IHX}	effectiveness of the Internal Heat Exchanger, –
η_b	burner thermal efficiency (LHV), –
$\eta_{a\rightarrow p}$	air-to-product heat transfer efficiency, –
η_{is}	isentropic compressor efficiency, –
$\eta_{HX,evap}$	air-side heat exchanger efficiency at evaporator, –
$\eta_{HX,cond}$	air-side heat exchanger efficiency at condenser, –
ω	acentric factor of the refrigerant, –
ρ	density, kg/m^3

Abbreviations

ATEX	ATmosphère EXplosible (EU Directive 2014/34/EU, equipment for explosive atmospheres)
CAPEX	Capital Expenditure
EoS	Equation of State
ETS	European Union Emissions Trading System
EU	European Union
GWP	Global Warming Potential (100-year horizon, IPCC AR5)
HCFO	Hydro-Chloro-Fluoro-Olefin
HFC	Hydro-Fluoro-Carbon
HFO	Hydro-Fluoro-Olefin
HTHP	High-Temperature Heat Pump
IEA	International Energy Agency
IHX	Internal Heat Exchanger
LCOH	Levelized Cost of Heat
LHV	Lower Heating Value
OEM	Original Equipment Manufacturer
P&ID	Piping and Instrumentation Diagram
PV	Photovoltaic
R1233zd(E)	trans-1-chloro-3,3,3-trifluoropropene (HCFO refrigerant)
R1336mzz(Z)	cis-1,1,1,4,4,4-hexafluoro-2-butene (HFO refrigerant)
R601	n-pentane (natural hydrocarbon refrigerant)
SPES	Specific Primary Energy Saving